Royal Netherlands Institute for Sea Research

This is a pre-copyedited, author-produced version of an article accepted for publication, following peer review.

van Leeuwen, S.M.; Beecham, J.; García-García, L.M.; Thorpe, R. (2022). The Mediterranean Rhodes Gyre: modelled impacts of climate change, acidification and fishing. *Mar. Ecol. Prog. Ser. 690*: 31-50.

Published version: https://dx.doi.org/10.3354/meps14016

NIOZ Repository: http://imis.nioz.nl/imis.php?module=ref&refid=352714

[Article begins on next page]

The NIOZ Repository gives free access to the digital collection of the work of the Royal Netherlands Institute for Sea Research. This archive is managed according to the principles of the Open Access Movement, and the Open Archive Initiative. Each publication should be cited to its original source - please use the reference as presented.
When using parts of, or whole publications in your own work, permission from the author(s) or copyright holder(s) is always needed.

The Mediterranean Rhodes Gyre: modelled impacts of climate change, acidification and fishing

Running page head: Rhodes gyre future biomass levels

Sonja M. van Leeuwen[1,2,*], Jonathan A. Beecham[2], Luz M. García-García[2,3] , Robert Thorpe[2],

[1] NIOZ Royal Netherlands Institute for Sea Research, department of Coastal Systems,, and Utrecht University, 1797 SZ, 't Horntje, Texel, The Netherlands
[2] Centre for Environment, Fisheries and Aquaculture Science, NR33 0HT, Lowestoft, United Kingdom
[3] Spanish Oceanographic Institute, 15001 Coruña (A), C, Spain
[*] corresponding author: sonja.van.leeuwen@nioz.nl

ABSTRACT: The Mediterranean Rhodes gyre is a cyclonic gyre with high primary production due to local upwelling of nutrients, and occasional deep overturning up to 1km depth. This nutrient-rich state is in sharp contrast to other parts of the Eastern Mediterranean which are oligotrophic. Here we study the upwelling system central to the Rhodes gyre and the impact of different stressors like meteorological changes, acidification and fishing pressure up to the year 2100. A water column model spanning the physical, chemical and biological system up to top predators (GOTM-ERSEM-BFM-EwE) was used to simulate the pelagic environment under single and combined stressors. Results show that due to increasing winter temperatures deep overturning events are becoming more rare in the future, until they stop occurring around 2060 under the business-as-usual climate scenario (RCP8.5). Stratification becomes stronger as temperature effects outweigh salinity effects in the surface mixed layer. Together with the lack of deep overturning this limits the nutrient supply to the euphotic zone, significantly reducing primary production. Phytoplankton species shift towards smaller species as nutrients become more scarce, mimicking the situation found currently on the edge of the gyre. Climatic changes and fishing pressure affected higher trophic levels in an additive way for some species (sardines, dolphins), while in a synergistic way for others (anchovy, mackerel). Acidification impacts were negligible. Fish stocks reduced significantly under both climate scenarios: ~30% under RCP4.5 and ~40% under RCP8.5, with limited beneficial impact of MSY-level fishing, indicating a need for mitigating measures beyond fleet control.

Keywords: Rhodes gyre; ecosystem modelling; climate change, fishing pressure, ERSEM, Ecopath with Ecosim

1 Introduction

The Mediterranean Sea is the largest and deepest semi-enclosed sea on Earth, and has a long history of providing ecosystem services (Colonese et al. 2010). It is a biodiversity hotspot and has strong west-east gradients in temperature, salinity and productivity, with the Eastern Mediterranean basin exhibiting higher sea surface temperatures, higher salinity and lower productivity than the western part (Coll et al. 2010). As such, the Eastern Mediterranean supports little biomass compared to other (semi)-enclosed seas (Salihoglu et al. 1990, Vidussi et al. 2001). Within this system the Rhodes gyre forms an exception: due to the local topography and the cyclonic nature of the gyre upwelling occurs in its center, pushing nutrient-rich bottom waters upwards to within reach of the euphotic zone. This results in a high production area in the otherwise oligotrophic Levantine basin (Siokrou-Frangou et al. 2010), which is further characterized by narrow continental shelves. In terms of the types of fisheries the Rhodes gyre is part of the Aegean Sea geographical subarea (Colloca et

al. 2017), making it difficult to estimate its importance separately. Nevertheless, Megalofonou & Damalas (2012) show the Rhodes gyre is an important area for Swordfish catches. In general, Mediterranean stocks are overexploited (Colloca et al. 2010). Threats facing the Mediterranean's unique ecosystem include habitat degradation, climate change, eutrophication, pollution and invasive species, amongst others (Galil, 2009, Coll et al. 2010).

The Mediterranean ecosystem is deemed to be particularly vulnerable to climatic changes (Giorgi & Lionello 2008, Cramer et al. 2018). Shaltout and Omsted (2014) show that the Levantine basin and the Black Sea are the fastest warming basins under the CMIP5 scenarios (Coupled Model Intercomparison Project Phase 5, providing regional climate predictions to 2100) in the Mediterranean, with current surface temperature increases of 0.042 ^{o}C yr^{-1} and 0.51 ^{o}C yr^{-1} respectively (based on 1982-2012 observations, the Active Atlantic Mediterranean displays the lowest increase with 0.024 ^{o}C yr−1) and an expected increase of 2.5 ^{o}C by 2100 under the worst case emissions scenario (business as usual or RCP8.5, relative to predicted 2000-2029 temperatures). Within the Levantine basin, the Rhodes gyre experiences exceptional warming, particularly in average sea surface temperature and mean winter surface temperature. It is therefore important to gauge how this will affect the upwelling and overturning mechanism and associated Rhodes gyre productivity.

To this end we perform a multi-stressor modelling study of the Rhodes gyre system, simulating responses up to 2100. We apply a coupled ecosystem model to the area, simulating the vertical water column physics (temperature, salinity, currents, etc.), chemistry (nutrient cycling, pH, etc.), lower trophic levels (organisms that are moved by the currents) and higher trophic levels (organisms that can swim). Bottom-up stressors like acidification and climate change are imposed alongside the top-down stressor of fishing in this deep, offshore location. This way, indications of system changes can be identified, and consequences for economically important species gauged, which can focus further studies and/or management strategies.

2 Method

2.1 Area description and model location

The Eastern Mediterranean is characterised by 2 large gyres, comprising several smaller ones (Figure 1). The anti-cyclonic gyre in the southern Levantine basin comprises the Mersa-Matruh and Shikmona gyres, while the cyclonic gyre in the northern Levantine basin encompasses the Rhodes gyre and West Cyprus gyre. Of these, the Rhodes gyre is a permanent feature which causes continuous upwelling of water in its centre from deeper layers containing Levantine Deep Water (LDW). This process is driven by the local topography, the wind-driven circulation and interaction of 2 local currents (Mid-Mediterranean Jet, Asia Minor Current) (Gaines et al. 2006). The surface mixed layer (SML) within the Rhodes gyre has a depth of 25-75m and mixes with the layer below (up to 150 to 200m deep) to form Levantine Intermediate Water (LIW): the area is considered to be the main formation point of LIW (Lascaratos et al. 1993, Pinardi and Masetti 2000, Menna & Poulain 2010). Levantine Intermediate Waters are deemed to control deep water formation in the northern Mediterranean areas (Wu & Haines, 1996) and contribute predominantly to the Gibraltar-Atlantic flux (Robinson et al. 2001). However, Kubin et al. (2019) estimate that most LIW is formed in coastal currents in the area, and that the Rhodes gyre is more important as a formation area of LDW during strong convection events.

The central upwelling causes the Rhodes gyre to be one of the most productive areas of the Mediterranean Sea (Vidussi et al. 2001), and an important high production area in the Eastern Mediterranean, which is otherwise an oligotrophic area (Ediger and Yilmaz 1996, Siokou-Frangou et al. 2010, Powley et al. 2017, Teruzzi et al. 2018). In general, the Eastern Mediterranean is

characterized by high nutrient bottom waters at large depths and nutrient-depleted surface waters with a nutricline well below the euphotic zone. However, in cyclonic gyres upwelling occurs in the center which pushes the nutricline upwards: in the Rhodes gyre Levantine Deep Water (LDW) is pushed upwards to a depth of around 150-200m. The euphotic depth in these clear, offshore Mediterranean waters is around 70-100 m (Soikrou-Frangou et al. 1999, Ediger et al. 2004), and within the Rhodes gyre the nutricline is pushed up to 50-125 m depth (Ediger et al. 2004), thus reaching the base of the euphotic zone. This leads to nutrients being introduced into the productive zone from the nutricline by vertical mixing, especially in winter months when thermal stratification is minimal (Siokou-Frangou et al. 1999). Primary production mainly occurs in a deep chlorophyll maximum at the base of the euphotic zone.

However, in years with strong evaporation and, in particular, long cold winters the combined effect of saltier, colder water than normal at the surface can cause overturning of the water column. The the top layer (first 150-200m) becomes more dense than the LDW below and the heavier water sinks, causing a complete remixing of the water column up to 1000 or more meters. This remixing allows for the nutrient rich waters of the LDW to reach the surface and cause a plankton bloom where the upwelling nutrients reach the photic zone (Ediger and Yilmaz 1996, Malanotte-Rizzoli et al. 1999, Ediger et al. 2005, Yilmaz et al. 2007). These overturning years are characterized by high nutrient concentrations within the surface layer (NO_3: 4.7±0.4 μM, PO4 0.16±0.02 μM and Si 7.8±0.4 μM), matching LDW values. The area is deemed to be generally phosphate limited (Yilmaz et al. 2007).

Phytoplankton species within the Rhodes gyre center are dominated by diatoms, dinoflagellates and cocolithophores (Siokou-Frangou et al. 1999), i.e. large species that benefit from the high nutrient concentrations. Chlorophyll-a concentrations and primary production values can be as high as 3 mg m^{-3} and 1.1 g C m^{-2} d^{-1} respectively, in the Rhodes gyre in years experiencing deep overturning (Yilmaz et al. 2007). Vertical diel migration of zooplankton is largely absent in the North Levantine basin, and could be due to the absence of strong migrants such as copepods, with the Rhodes gyre exhibiting a relative low abundance of copepods and high abundance of Appendicularians (Mazzochi et al. 1997). For an overview and species information on plankton in the Rhodes gyre and wider area see Siokou-Frangou et al. (2010).

2.2 Hydrodynamic model setup

The model location for the Rhodes gyre simulations was chosen as [35.75 °N, 28.6 °E], which has a local depth of 4088 m. However, as we apply a water-column model the three-dimensional processes which cause the center of the Rhodes gyre to shift spatially each year are not represented here. The chosen model location will therefore always represent the center of the Rhodes gyre, rather than a fixed geographic location. Due to the large depth we do not include the seabed or any related benthic organisms and processes.

A 1 dimensional vertical setup was used (1DV or water column model), as the main processes are vertically oriented and the reduced simulation time (compared to a laterally explicit setup) allows for many simulations to be carried out, making it suitable for a multi-stressor study. We used 120 vertical (sigma) layers to simulate to 1000 m depth with increased resolution at the surface, and excluded the sea bed and associated dynamics due to the large depth. Layer width ranged from 1 to 2 m near the surface to 14.6 m at around 660 m depth, decreasing again to ~ 11m at 1000m depth. The hydrodynamical model used was GOTM (General Ocean Turbulence Model), an open source model available from github (www.gotm.net).

In order to simulate the dominating physical process of upwelling and occasional overturning the water column model was relaxed towards constructed temperature profiles which impose the observed layered structure of SML, LIW and LDW (i.e. the model solution was nudged towards the

profiles but not forced to be identical). These profiles were based on ICES CTD data (see section S3.2) and dependent on air temperature to account for changing meteorological conditions. As temperature, salinity and thus density are calculated by the model depending on the atmospheric conditions (including evaporation) it was able to simulate deep mixing in years with long, cold winters. We used Jerlov Type I waters. Tidal constituent data for the given location were obtained from Topex/Poseidon , representing weak M_2 and K_1 tides. Waves were not accounted for.

2.3 The lower trophic level model

The marine chemistry and lower trophic levels of the ecosystem were simulated using the ERSEM-BFM model (www.nioz.nl/en/about/cos/ecosystem-modelling/ersem-bfm-model). This model was constructed by NIOZ and Cefas institutes from the BFM model (Biogeochemical Flux Model, Vichi et al. 2013), which is the modern version of the original ERSEM model (European Regional Seas Ecosystem Model, Baretta et al. 1995). The ERSEM-BFM model was further developed to include an extensive benthic compartment, but this is not used here. Organisms in ERSEM and ERSEM-BFM have internally varying nutrient ratios (i.e. not defined by the Redfield ratio), allowing for luxury uptake of nutrients. Additional pelagic development to ERSEM-BFM consists of TEP production by nutrient-stressed diatoms (Transparent Exopolymer Particles which causes macro-aggregate formation,resulting in rapid sinking out of a diatom bloom) and the addition of nitrifying archaea and *Phaeocystis*, a colonial nuisance algae. As a result, the applied model comprises 6 functional groups for phytoplankton (diatoms, flagellates, picophytoplankton, dinoflagellates, resuspended benthic diatoms, *Phaeocystis* colonies), 5 for zooplankton (heterotrophic nanoflagellates, microzooplankton, omnivorous mesozooplankton, carnivorous mesozooplankton, filter feeder larvae) and encompasses pelagic bacteria besides archaea (nitrifying bacteria). All zooplankton groups (except filter feeder larvae) experience cannibalism, to mimic biomass-dependent grazing by higher trophic levels. A schematic overview of the model is given in Figure 2. Iron (Fe) was added as an extra nutrient, and integrated in the nutrient cycling, including speciation in Fe-II and Fe-III (the speciation is pH dependent, providing another way for the acidification stressor to impact on ocean chemistry). However, as this open ocean site is not iron limited due to the high amounts of Saharan dust deposition (Zhang et al. 2015) we do not expect this to influence results much. Examples of application of this model (without Fe) in water column stressor studies are van der Molen (2013) and van Leeuwen (2015), which present model validation but apply different future meteorological forcing. Derived Fe deposition values are provided in the supplementary materials, Table S1.

2.4 The higher trophic level model

The Ecopath with Ecosim (EwE) model was originally developed at NOAA with the main subsequent development occurring at the University of British Columbia (Christensen & Pauly 1992, Steenbeek et al. 2015, www.ecopath.org). Here, the Ecopath model describes the static food web, while Ecosim provides the temporal development of the static system in response to external, time-varying, drivers. Applications of EwE in the eastern Mediterranean hardly exist (Coll & Libralato 2012), and none are specific to the Rhodes gyre or offshore cyclonic areas. Therefore, we based the representation of higher trophic levels upon the Aegean Ecopath with Ecosim model (Tsagarakis et al. 2010) with the benthic components removed, as illustrated in Figure 2. S Species discarded from the model by Tsagarakis et al (2010) were: benthic small crustaceans, polychaetes, shrimps, crabs, Norway lobster, benthic invertebrates, octopuses & cuttlefish, red mullets, anglerfish, flatfishes, other gadiformes, demersal fishes 1-4, demersal sharks and demersal rays & skates. Those retained are given in Table 1.

The main targeted species are sardine (*Sardina pilchardus)* and anchovy (*Engraulis encrasicolus)*, with limited additional effort targeting mackerels (*Scomber japonicus, S. scombrus)*, picarels and bogues (*Boops boops, Spicara maena, S. smaris)*, hake (*Merluccius merluccius)* and medium and small pelagics (Tsagarakis et al (2010)). The original model incorporated five fishing fleets, of which 3

were artisanal (static nets, longlines and troll baits, cephalopod pots) and 2 commercial (bottom trawls and purse-seines). As the Rhodes gyre is far offshore with depths > 4000m we eliminate the artisanal fleet effort (too far) as well as the bottom trawls (too deep), limiting the imposed fleet to the commercial purse-sein fisheries.

2.5 Coupling

The lower and higher trophic level models were coupled one-way upwards, i.e. biomass fields from ERSEM-BFM were used as input into the food web model.

All edible phytoplankton groups were linked to the EwE phytoplankton (apart from resuspended benthic diatoms and *Phaeocystis*, which did not survive in this offshore location). Bacteria and detritus were not coupled to give each model its own regeneration cycle. Biomass time series of phytoplankton (diatoms + flagellates + picophytoplankton), ciliates and mesozooplankton were calculated by GOTM-ERSEM-BFM and provided realtime to the EwE model via the CouplerLib model coupler (Beecham et al. 2016). Unfortunately, two-way coupling proved elusive within the project time. Thus, EwE calculated biomass fields (and fishing pressures) did not feed back into the lower trophic level model. Climate change and acidification pressures did impact on higher trophic levels through the lower trophic level biomass time series and surface mixed layer temperature values. The latter replaced the ambient background temperature in EwE.

2.6 Scenarios

The Mediterranean is a hotspot for climate change effects, with the Levantine basin and the Black Sea the most impacted regions (Giorgio & Lionello 2008, Shaltout et al. 2014, Cramer et al. 2018). Here we consider two projections of the IPCC (2014) report: representative concentration pathway (RCP) 4.5 (an intermediate emission scenario akin to observance of the Paris agreement) and 8.5 (a high emissions scenario assuming business as usual). The associated atmospheric pCO_2 concentrations are shown in Figure S2**Error! Reference source not found.**. All stressors were applied at two different levels to accommodate climate projection uncertainties and to encompass different management options. Results of this work were made available to marine managers in a decision support tool (de Kok et al. 2016).

For this multi-stressor study we consider two bottom-up pressures (climate change and ocean acidification, denoted as CC and OA respectively) and one top-down pressure (fishing, denoted as F). Each stressor was applied at two different levels, and combinations of the different stressors were also simulated (Table 2). The acidification pressure was applied by direct forcing of the lower trophic level model with the atmospheric pCO_2 values (Figure S2**Error! Reference source not found.**): this affects the CO_2 exchange at the atmospheric-ocean boundary. The carbonate chemistry within ERSEM-BFM is based on the code by Dickson in DOE (1994), and considers CO_2, HCO_3^-, CO_3^{2-}, pCO_2, pH , DIC and total alkalinity (TA) as state variables (see also Vichi et al, 2013, the carbon module is the same as in the applied model). Biological production of CO_2 through respiration is standard for all functional groups, while consumption of CO_2 through photosynthesis is included for phytoplankton only, including limitation of primary production by the HCO_3^- concentration. The latter allows for pH changes to affect the primary productivity, as lower pH values will result in higher HCO_3^- concentrations (potentially relieving DIC limitations on production). Phytoplankton production is dependent upon the light availability, temperature and nutrient limitation, with CO_2 uptake to equal the possible production. Respiration is the total of basal respiration and activity respiration. The first is a function of temperature and carbon biomass while the latter is a constant fraction of the gross primary production (species dependent fraction). During the spring bloom CO_2 uptake by phytoplankton significantly raises the local pH, due to the formation of H^+ ions. Scenarios OA1 and OA2 refer to the application of the RCP4.5 and RCP8.5 atmospheric pCO_2 concentrations, respectively.

The associated meteorological conditions at the model location are shown in Figure S2, supplementary materials, and were obtained by interpolation from the Coupled Model

Intercomparison Project phase 5 (CMIP5, Taylor et al. 2012). CMIP5 is part of the Cordex program (Coordinated Regional Climate Downscaling Experiment, see http://cordex.org/). Here we used an ensemble run- (r1i1p1) of the Regional Climate Model CMCC-CCLM4-8-19, run by the Euro Mediterranean Centre on Climate Change (CMCC) and forced at the boundaries with the Global Climate Model CMCC-CM. The spatial resolution of this product is 0.44 degrees (~50km) and the temporal resolution is 1 day. The data consisted of (daily-averaged) wind speed (m/s) and direction (degrees from North), humidity (%), air pressure (hectoPascal), dry air temperature (at 2m, ^{o}C) and cloud cover (fraction 0-1). The air temperature is expected to increase by 4.5 ^{o}C over the 21st century under the RCP8.5 scenario. A slight decrease in cloud cover and wind speed is also predicted for the Rhodes gyre area. These meteorological conditions were applied to the hydrodynamic model GOTM and constituted the climate scenarios CC1 (RCP4.5) and CC2 (RCP8.5).

Finally, fishing pressure was applied in a low (LF) and high (HF) level compared to the default fishing pressure in the food web model of a commercial purse-sein fleet targeting mostly anchovy and sardines (see section 2.4). Low and high levels refer to 0.5 and 2 x the level imposed by Tsagarakis et al. (2010) (their Table 1), respectively, with reference fishing pressures (ratio of fished biomass over total biomass for a species, i.e. the fraction of fish removed by fishing) of 0.25 yr^{-1} (adult anchovies) and 0.42 yr^{-1} (adult sardines). Note that anchovy initial biomass is double that of sardines in the model, so that anchovy dominate the total catch. As most Mediterranean stocks are overfished (FAO 2018), the reference conditions are expected to be higher than MSY (maximum sustainable yield) levels. Specific values for sardines and anchovy in the Aegean subarea (which includes the Rhodes gyre) were not provided in FAO (2018), but general Mediterranean overfishing estimates (F/F_{MSY}) were 2.0 and 1.7 respectively. Thus, the low fishing pressure scenario used here can be seen as close to MSY levels for these species.

Table 2 shows the different scenarios applied in the study. Note that not all possible combinations were used: as both climate change and acidification are driven by the same increases in atmospheric pCO_2 levels we did not mix these pressures (only including CC1OA1, CC2OA2 as combinations). The single pressures were used (CC1, OA1, CC2, OA2) to gauge individual stressor impact and aid interpretation of the multi-stressor experiments. They also aligned with mesocosm studies within the wider project (Ocean Certain), using Cretan Sea waters (see Hopwood et al. 2020). As the models were linked one-way upwards the fishing pressure was only applied to the higher trophic level model. As such, 7 simulations were performed for the lower trophic levels and 17 for the higher trophic levels. All scenario simulations were started from the equilibrium state provided by the initial 1958-2099 reference simulation. A separate simulation over 1958-2014 was performed with the realistic ECMWF ERA-Interim forcing for validation purposes. See section S1 for a comparison between the ECMWF and the CMIP5 meteorologies.

The coupled model simulated the period 1958-2099 (as the meteorological forcing conditions were not complete for the year 2100). To analyse long term trends we mainly consider results in 30-year averages (Table 3) in order to filter out inter-annual and decadal variations and match the repeated climate period of the reference simulation.

3 Results

3.1 Validation

Comparison of model results with observations requires a realistic meteorological forcing since the applied CMIP5 meteorological forcing does not guarantee to reproduce actual observed historical events (Taylor et al, 2010), even in the historical experiment. Thus we do not expect the model to simulate overturning in the years that it has been observed (e.g. 1992, 1993 and

1995,Yilmaz et al, 2007). Instead, the model will predict the marine changes associated with changes in the frequency of the overturning. The difference between the validation simulation (ECMWF forcing) and the reference scenario (CMIP5 forcing) for sea surface temperature shows summer temperatures in the reference run are ~ 2°C lower than those of the validation run, which reflects the differences in the meteorological forcing (Figure 3a). Modelled SST was compared to satellite observations from the Mediterranean Sea high resolution and ultra-high-resolution Sea Surface Temperature Analysis, processed by the CNR-ISAC-GOS (Consiglio Nazionale delle Ricerche, Istituto di Scienze dell'Atmosfera e del Clima - Gruppo di Oceanografia da Satellite, Italy) and obtained from Copernicus Marine Environment Monitoring Service (CMEMS, https://marine.copernicus.eu/) . The Taylor diagram in Figure 3b shows that both model results are similar in correlation and error with respect to the observations, although the validation run overestimates the standard deviation, whereas the reference run underestimates it. See section S1 for a longer period of comparison for air temperature and wind between the two applied meteorology's and section S5 for additional model validation.

Nutrient data for the Rhodes gyre centre are limited, and the observational values in Yilmaz et al (2007) were used to define LDW concentrations within the model. The simulated surface values in standard, non-overturning years were ~0.7, 10.0, 0.02 (NO_3, Si, PO_4), while in overturning years this changed to ~ 4.7, 6.5, 0.24 (NO_3, Si, PO_4). Note that in our simulations the surface silicate concentrations (fed by constant atmospheric deposition of Saharan sands) decrease in deep overturning years due to the enhanced primary production. Surface nitrate and phosphate concentrations match those observed for both standard and deep overturning years (see section 2.1) as reported by Yilmaz et al (2007). Other sources report nitrate concentrations of 5.0 µM (Vidussi et al, 2001) and 5.5 µM (Ediger & Yilmaz, 1996) in the surface layer during overturning events. Maximum simulated chlorophyll-a concentrations in deep overturning years were ~ 5 mg Chla m^{-3}, while maximum net primary production rates were 3-4 $gCm^{-2}d^{-1}$. This refers to the period of 1978-2008 and the maximum over the whole water column, and shows elevated values compared to those reported by Yilmaz et al (2007) (see section 2.1, covering 1992-1995). This is likely caused by the slightly higher PO_4 and higher Si concentrations in our simulations: with PO_4 the limiting nutrient any increase there will increase primary production. The study presented here focusses on long-term, averaged impacts and the model is able to capture the observed phosphate limitation, production at depth and deep overturning events, as well as nutrient concentrations and primary production in the right order of magnitude. As such, we believe the model is capable of predicting future changes to the Rhodes gyre ecosystem.

3.2 Physical and chemical changes

The simulated Rhodes gyre stratification increases strongly under future climes, due to increased air temperatures and higher sea surface temperatures (Figure 4a,b). Ocean acidification has no discernable impact on the vertical structure, with the OA1, OA2 scenarios coinciding with the reference simulation. The physical impact of higher air temperatures and the resulting increased stratification and decline in cold winters can be seen in the maximum annual PO_4 concentrations at the surface (Figure 5): in the reference simulation LDW values of PO_4 reach the surface occasionally throughout the 20th century. Under the Paris agreement (RCP4.5, CC1) scenario surface PO_4 values do not reach LDW values anymore after the 2060's, indicating that overturning has stopped. For the business-as-usual scenario (RCP8.5, CC2) overturning does not occur anymore by 2040. Surface PO_4 values decrease steadily with increasing air temperatures as vertical mixing at the LDW/LIW and LIW/surface layer interfaces is reduced. This results in much lower nutrient concentrations in the euphotic zone in non-overturning years.

CO_2 uptake by the ocean is mainly governed by ocean acidification impacts, with a smaller contribution from climatic changes: acidification causes an increase in dissolved inorganic carbon (DIC)

and a decrease in pH values within the water column, which are slightly modified by climatic changes. The combined stressors impact seems synergistic: for stronger stressor impact the mitigating effect from climate changes increases. Note that in the reference simulation the surface DIC and pH values also change over time: the system needs to adjust to a new equilibrium with the imposed constant 2008 atmospheric pCO_2 values. Changes in primary production can also influence pH values, as photosynthesis uptake of CO_2 increases the local pH. As such, the observed changes in simulated DIC and pH in the water column are the result of both chemical and biological changes in the system.

3.3 Response of the lower trophic level system

Future lower PO_4 levels in the surface mixed layer, as a result of reduced vertical mixing and lack of deep overturning, have a strong impact on the biological system: net primary production decreases sharply (Figure 4**Error! Reference source not found.**e, CC1: -23%, CC2 -30%), as does carbon export to below 90 m depth (Figure 4f, considered long-term carbon storage, CC1: -19%, CC2: -23%). The surface mixed layer changes from a phytoplankton dominated system to a bacteria dominated system (Figure 4g), while the planktonic system changes from a phytoplankton dominated one to a zooplankton dominated one (Figure 4h). Available fish food (depth-integrated biomass of all ERSEM-BFM functional groups that are used as input for the EwE model) also decreases sharply (Figure 4i).

The biological changes of the different functional groups (Figure 6) are completely dominated by climate change impacts (scenarios CC1, CC2, CC1OA1, CC2OA2), due to the large physical changes in the system under future, warmer climes. Depth-integrated biomass decreases significantly over all groups, with phytoplankton (CC1: -33%, CC2: -39%) and zooplankton (CC1: -30%, CC2: -35%) affected more strongly than bacteria (CC1: -15%, CC2: -17%), which remain largely unaffected below the surface mixed layer. The reduced nutrient levels in the euphotic zone benefit the smaller picophytoplankton, which are better at nutrient uptake in low nutrient conditions. The large percentage reduction in diatoms in both climate scenarios is only matched for flagellates in the higher impact climate scenario (CC2, Figure 6), as flagellates are still able to take over the spring bloom in the CC1 scenario (results not shown). Simulated biomass values decline for all phytoplankton groups with diatoms the most affected (Figure 7a). Phytoplankton community structure changes as a result, with picophytoplankton contribution nearly equaling diatom contribution by 2100 at the cost of flagellates and dinoflagellates (Figure 7c). Diatom contribution initially declines as the climate warms, with flagellate contribution increasing, but is back to nearly pre-scenario percentages by the end of the century. Dinoflagellates disappear altogether in the climate scenario simulations. Heterotrophic nanoflagellates (HNAN) feed predominantly on bacteria and picophytoplankton, yet only ciliates (which feed on HNAN) benefit enough to increase their biomass under future climes (Figure 6c, Figure 7b,d).

The 30-year averaged seasonal signal for phytoplankton functional groups (surface layer, Figure 8) under the full RCP8.5 scenario clearly shows the decline in the larger species (diatoms and dinoflagellates, which are microphytoplankton) in the top mixed layer, with picophytoplankton (the smallest function group) benefitting. At nutricline depth the change is less dramatic (results not shown), with diatoms reducing in biomass but still able to dominate the spring bloom. Here the increased stratification inhibits mixing upwards of nutrients, whereas at the surface layer the lack of deep overturning causes nutrient levels to collapse.

3.4 Response of the higher trophic level system

The Rhodes gyre region is a deep water site, where the pelagic fisheries mainly target sardine and anchovy. These small pelagic fish feed on meso- and microzooplankton, and are food for medium-sized fish such as mackerel and a few larger predators such as hake, squid, and dolphins (Figure 2). Climate change impacts on the lower trophic levels show reduced biomass levels for phyto and zooplankton, and a decline in the food available for the local higher trophic level food web (Figure 4i).

In particular mesozooplankton (omnivorous and carnivorous) declined strongly (Figure 6c), leading to a bottom-up controlled decline in pelagic stocks in around 40-60 years from now (Figure 9a,b). Anchovies show a strong decline even with the RCP4.5 climate scenario (CC1) of ~26% by 2100 (Table 4), which increases to 40% under the RCP8.5 scenario (CC2) under low fishing pressure. Sardine stocks depict a similar development, with biomass losses of ~30% (CC1) and ~38% (CC2) under low fishing pressure. Both stocks show signs of stabilization by the end of the 21st century. Mackerel biomass (Figure 9c) shows a similar pattern, but with less distinction between the two imposed fishing scenarios as a less targeted species (Table 4). Again, the major change occurs already under the medium emissions scenario of CC1 (Paris agreement). Decreases in the productivity of the pelagic stocks have consequences further up the food chain, where dolphin numbers decline significantly (Figure 9d, Table 4): ~30% reduction under the CC1 scenario and ~40% reduction under scenario CC2.

Fishing pressure impacts are remarkably stable for sardines (~23% decline) and dolphins (~10% decline), regardless of the climatic stress level indicating an additive response. Anchovy numbers show signs of synergistic response of combined climate and fishing pressure, with the addition of climate stress adding a ~10% decline to biomass stocks. Mackerel biomass levels increased with increasing fishing effort, due to a relaxation of predation on this species (mainly by medium and large pelagic fishes and dolphins) caused by climate change impacts. Acidification is not depicted separately as lower trophic level impact was negligible and there is no direct impact on higher trophic level for this stressor other than via planktonic biomass fields.

4 Discussion

4.1 Main findings

Cramer et al. (2018) show that the Mediterranean basin is warming faster than the global average. Within the basin, the Rhodes gyre is warming faster than other areas, in particular winter sea surface temperatures (Shaltout and Omsted 2014, Skliris et al. 2012), which will suppress the occasional deep overturning. Here we examined the impact of these changes on the ecosystem in the center of the Rhodes gyre. The presented results show that the system is very sensitive to climatic changes, not very sensitive to ocean acidification impacts and that fishing pressure can be seen as an additive stressor. Physically the vertical structure in the 1DV model is determined by the surface heat exchange. Increased air temperatures increase the surface mixed layer (SML) temperature, decreasing SML density, while increased evaporation (mainly due to increased air temperatures) increases surface salinity (increasing SML density). Overall, the density of the surface layer decreases under future climes in our simulations (Figure 4b), indicating the lack of cold winters being the main driver for the decline and eventual cessation of deep overturning events (Figure 4a, Figure 5). As such, the temperature effect is dominant here over the salinity effect. The local ecosystem is reliant upon the continuous upwelling and the overturning events, which cause nutrient rich LDW waters to reach the surface layer. In our simulations, deep overturning stops occurring between 2040 (CC2 or RCP8.5, business-as-usual emissions scenario) and 2060 (CC1 or RCP4.5, Paris agreement emissions scenario)(Figure 5). Without these deep overturning events the surface nutrient concentrations drop sharply and primary production declines by 23-30% (CC1-CC2 respectively, Figure 4e). Phytoplankton community structure shifts to smaller species (Figure 7a,c, Figure 8) and the diatom spring bloom collapses in near-surface waters (Figure 8). Flagellates take over this spring bloom under the moderate climate scenario (CC1, results not shown) but fail to do so under the worst-case climate scenario (CC2, Figure 8). Diatoms maintain the spring bloom only close to the nutricline layer, in the model varying between 75-150m depth in these clear offshore waters (see Figure S5 for thermocline depth and Figure S6 for halocline depth). The surface mixed layer displays a shift to a bacteria and zooplankton dominated system (Figure 4g,h), indicating an increased importance of the microbial loop (pelagic bacteria-heterotrophic nanoflagellates (HNAN)-dissolved organic material). The HNAN decrease in absolute biomass numbers, but remain the

largest zooplankton group (Figure 7b,d). Ciliates (microzooplankton) are the only plankton functional group to increase their biomass under the climate scenarios (Figure 6c, Figure 7b). This is likely due to the reduction in grazing pressure from mesozooplankton on ciliates, indicating top-down control within the lower trophic level model on HNAN and ciliates. Mesozooplankton declines strongly as their main food source diatoms declines: the relatively small increase in their second food source (ciliates) cannot compensate for this (Figure 7).

The decline in plankton biomass results in a strong biomass decline at higher trophic levels, with stabilization only towards the end of the 21st century. Economically important species like anchovies and sardines decline with ~30% (CC1) and ~40% (CC2) under low fishing pressure, which is deemed close to MSY levels. Current fishing levels are higher than this, indicating the need for strong management action to limit significant climate change impacts on commercial stocks under even a moderate impact scenario (RCP4.5). Combined fishing pressure and climate change response was additive for some species (mainly sardines, dolphins), but not for others, illustrating the need for more combined stressor studies in food web research.

4.2 Model limitations

The coupled model was applied here in a 1DV (water column) set up, that represents the gyre center. Physical validation (section S4) shows that the simulated thermocline is deeper than observed, indicating that primary production may be underestimated by the model. As the system is nutrient limited (as opposed to light limited) we believe this effect to be small. SML temperatures are generally overestimated by the model while SML salinities are slightly underestimated. Thus, modelled results both overestimate SML density (too low temperatures) and underestimate SML density (too low salinity). This may affect the timing reported here for overturning cessation. We do not expect it to impact on our conclusion that long-term average temperature effects are dominant over those of salinity changes, weakening surface density, which was also reported by Skliris (2014), Hermann et al. (2008), Somot et al. (2006) and Thorpe & Bigg (2000). Note that although the model represents the gyre center the observations may represent other parts of the gyre, due to its variable geographic location.

ERSEM-BFM is a process-based model that represents organisms as functional groups. Currently, it does not explicitly represent mixotrophs (plankton that can switch between autotrophy and heterotrophy). Instead, biomass reacts to the available food sources and experienced predation, so that any functional group will increase in biomass when the conditions are favourable. As such, results for dinoflagellates are uncertain. Vertical migration of planktonic groups is also not included. Both phyto- and zooplankton species are known to migrate to depth at night (Staker & Bruno, 1980, Olli, 1999, Wirtz & Smith, 2019). Without this process (phytoplankton descending at night to access nutrients) primary production estimates by the model are likely underestimates in the upper SML layers. Note that the model does allow for luxury nutrient uptake, and that primary production occurs mainly in the deep chlorophyll maximum in both the model and in observations (Ediger & Yilmaz, 1996). The reported decline in net primary production in the area under future, warmer, conditions occurs mainly in the SML. As such, this mechanism can mitigate some of the presented impact. Like mixotrophy, diel migration is on the list for future model improvements. The simulated shift to smaller species is to be expected as nutrient levels decline in the top layer in the center of the Rhodes gyre: observations show that the current, high-nutrient, center of the Rhodes gyre is dominated by microzooplankton, with the periphery dominated by increasingly smaller organisms, shifting from nanophytoplankton to picophytoplankton at increasing distance from the center as nutrient levels decrease accordingly (Vidussi et al. 2001). We therefore do not expect mixotrophic dinoflagellates to be important in this area.

Ecopath with Ecosim (EwE, see www.ecopath.org) ” is a food web model based on species interactions. As such it relies on ecosystem knowledge of diets, biomass accumulation and detritus production rates, mortalities and respiration rates for all simulated groups. We adapted the existing

model of Tsagarakis et al (2010) designed for the Aegean Sea. As such, we might miss specific open ocean pelagic species that have a defined niche in the Rhodes gyre system, but are lumped here in Large pelagic fishes. The model also does not account for the arrival and possible establishment of alien species. This process, which can alter the food web significantly, is a major threat in the Eastern Mediterranean, which is characterised by Red Sea species entering the basin through the Suez Canal (Galil, 2012). To date these are mainly found along coastal and shelf areas, due to the large number of observations in those environments (see e.g. Galil et al. 2014, Katsanevakis et al. 2016, Mannino et al. 2017). Observations in deep, offshore areas like the Rhodes gyre are limited (Coll et al. 2010); as a result little is known about the presence of alien species in our area of interest. Simulated stock decline can also be mitigated by inward migration of stocks from more productive coastal areas. Temperature is included in EwE as variable ambient temperature derived from the hydrodynamic model. Rising sea water temperatures did not lead to significant changes in main food web structure here, as the response was dominated by the decline in available plankton. Within EwE the consumption over biomass ratio and mortality are temperature dependent (Christensen et al., 2005). Thermal ranges were not applied as EwE version 5 was used: version 6.5 (released 2016) does allow for thermal range setting which provides a better estimate of higher trophic level response to increasing temperatures (Serpetti et al. 2017).

Model coupling was performed one-way upwards. Two-way coupling was attempted using the Couplerlib model (Beecham et al. 2016) but failed to achieve a stable ecosystem. Mass conservation in both models during real time coupling was achieved during test runs, but failed to produce stable results over the long-term simulations. As such, fishing pressure impact on lower trophic dynamics was missing and plankton group biomass was more likely resource limited than predation limited. Observational evidence of marine systems suggest irregular occurrence of predation limitation (Reid et al 2000). Casini et al. (2008) determine threshold levels for planktivorous fish biomass that determine food or predation limitation in plankton, with removal of the top predator leading to large abundance of plankton-feeding fish and a shift to predation limitation of the planktonic system. Niiranen et al. (2013) considered climate, nutrient and fisheries pressures in a coupled model study for the Baltic (one-way upward coupling), showing that fishing pressure (cod) combined with nutrient pressure could lead to two different ecosystem states by 2100. High fishing and high nutrient loads resulted in a eutrophied system characterized by high abundance of planktivorous fish, while low fishing and low nutrient loads lead to higher abundance of top predators, lower levels of planktivorous fish and eutrophication equivalent to current levels. In our study the local economic effort is concentrated on planktivorous fishes, not top predators. As such, fishing pressure could have a significant impact on planktonic community structure, and should be taken into account in further studies. Anthropogenic nutrient input scenarios were not included here due to the offshore location and the dominance of the local nutrient source (upwelling of LDW): the simulated change in vertical mixing is expected to be the major driver affecting nutrient availability in this location, and as such our findings effectively relate to nutrient reduction scenarios. Thomas et al. (2017) argue that nutrient availability alters the optimum growth temperature of phytoplankton, leading to a synergistic response of combined nutrient and temperature stress on plankton. This effect (not accounted for in the LTL model) would lower future primary production predictions in the current study. Taherzadeh et al. (2019) apply a theoretical frame work showing how size-based grazing pressure by zooplankton combined with nutrient limitation can evolve over time from an antagonistic to a synergistic phytoplankton response. We do not expect this to impact on our results as we apply 6 phytoplankton and 4 zooplankton functional groups (including size-selective grazing by zooplankton) and only consider long-term (30 years) averaged results.

Uncertainties within the CMIP5 simulations affect the results presented here. The long-term simulations are based on assumed land cover changes and atmospheric conditions, providing a forced climate response. Taylor et al. (2012) state that “In the long-term simulations, however, the timing of individual unforced climate events will only by coincidence match observations”. Thus, this

study limits itself to investigating changes in the long-term averaged overturning frequency and associated ecosystem changes. The CMIP5 projections provide the only future climate projections up to 2100 on a global and regional scale, and were created by the world's leading climate modelling centers. It thus represents the best estimate for future climate conditions currently available, and was also used by Cramer et al. (2018) and Shaltout and Omsted (2014) for Mediterranean studies. We did not include possible future changes in atmospheric deposition of Saharan dust, which can enhance the availability of nutrients in offshore waters. The Levantine basin is rich in atmospheric deposition, due to the proximity of the Sahara (Zhang et al. 2015), yet the only productive area apart from shallow coastal areas is the Rhodes gyre due to its upwelling regime (Soikrou-Frangou et al. 2010). Thus, we expect impacts of increased or decreased atmospheric deposition to be minor. The Mediterranean's biological processes are controlled by nutrient availability (Macias et al. 2014a, Coll et al. 2009), and it's main source in the Rhodes Gyre is the upwelling and overturning mechanism.

4.3 Wider area

The Rhodes gyre area is deemed the dominant formation area for Levantine intermediate waters (LIW, Pinardi & Masetti 2001), which control deep water formation in the northern Mediterranean areas (Wu & Haines 1996) and forms the principal contribution to the flux from Gibraltar into the Atlantic (Robinson et al. 2001). As such, changes within the Rhodes gyre system could impact on other areas within the Mediterranean, including the western basin. The Mediterranean thermohaline circulation as a whole has experienced profound changes during the past 40 years, with the formation of Eastern Mediterranean Deep Water (EMDW) shifting from the Adriatic to the Aegean Sea (Eastern Mediterranean Transient or EMT, Roethers et al. 1996, Klein et al. 1999) and back again (Tanhua et al. 2013, Waldman et al. 2018). This geographical shift in EMDW formation is thought to have been induced by the cold winters of the early 1990's (Skliris 2014). Formation of the EMDW in the Aegean Sea is linked to increased density of the resulting deep water (Skliris 2014). Increased density of the resulting Levantine Deep Water would enhance the reported stratification within the Rhodes gyre, further limiting nutrient exchange. However, as strong winters are declining in the area (this study) a future shift in EMDW becomes increasingly unlikely. Mid-layer waters in the Mediterranean (< 1500 m) are also still becoming saltier, and thus denser (Skliris et al. 2014), indicating stratification across the Mediterranean is intensifying. Previous basin-wide model studies have reported mixed results: Thorpe & Biggs (2000) and Somot et al. (2006) report lower densities of the surface mixed layer across the Mediterranean (due to increased temperatures, resulting in increased stratification and a weakening of deep water formation and thermohaline circulation under future conditions), while Macias et al. (2015) and Moullec et al. (2019a) report higher densities in the SML (due to increased evaporation, resulting in decreased stratification and increased productivity, particularly in the Levantine basin). Comparison periods in Macias et al. (2015) were 2095-2099 versus 2015-2019, whereas the current study uses 2069-2098 versus 1979-2008. Whether these years are representative of the climate trend is not known, but a 30 year average is a more robust measure of long-term trends. Both Macias et al. (2015) and Moullec et al. (2019a) used regional climate model output to impose marine physical changes and as such did not account for possible changes to the basin-wide thermohaline circulation, despite the indications reported by Thorpe & Biggs (2000) and Somot et al. (2006). Besides modelling studies Barale et al. (2008) observed a decrease in surface chlorophyll in Seawifs data in the basin interior, which they attributed to more stable stratification and thus reduced vertical mixing of nutrients. Skliris (2014) notes that regional, short-term exceptions exist to this mechanism, related to overturning events following cold winters.

The current study emphasizes that vertical changes can be profound and should be taken into account in studies predicting future Mediterranean productivity. Upwelling in the Rhodes gyre center is driven by the wind-driven circulation, the local topography and the interaction of the Mid-Mediterranean Jet and the Asia Minor Current (Gaines et al. 2006). As such, upwelling is expected to continue in the area, as well as formation of LIW (though its characteristics may change). The future

status of stratification determines future deep water formation and thus the thermohaline circulation in the basin. In general deep water formation is expected to decrease, due to decreased density of the surface layer, weakening the Mediterranean thermohaline circulation and reducing primary production (Skliris 2014, Hermann et al. 2008, Somot et al. 2006, Thorpe & Bigg 2000). This corresponds to the results found in the presented study focussing on the Rhodes gyre system. Note that coastal areas can experience high degrees of eutrophication and may exhibit increased primary production as a consequence, due to riverine and direct discharge nutrient loads.

Gyre response in general to future, warmer conditions will depend on regional characteristics. The Mediterranean experiences enhanced salinity changes due to the enclosed nature of the basin. Fresh water input into the basin has been reduced by more than 50% since 1950, mainly through dam construction (Poulos & Drakopoulos 2001). As such, the Mediterranean response might be dampened by the increased salinity impact (increasing surface density), as suggested by Skliris (2014). The current study suggests this is not the case for the Rhodes gyre system. Open ocean gyres are more likely to be driven solely by surface layer temperature increases, weakening vertical mixing and reducing primary production: this has already been observed for the North Atlantic gyre (D'Alelio et al. 2020). Arctic gyres are likely to face improved light conditions due to ice retreat, resulting in stronger stratification (lower surface salinity) combined with improved primary production (Beaufort gyre, Ji et al. 2019), at least in the short term. Letscher et al. (2016) argue that subtropical gyre primary production depends on both vertical and horizontal nutrient transport.

Reduction in primary productivity will inevitably lead to decreased biomass at higher trophic levels in these systems. The impact on a cyclonic, highly productive gyre system was studied here, and showed strong declines in commercial fish biomass despite mitigating impacts from increased surface salinity. Other gyre systems should therefore be studied with regional models to estimate their response to future climatic conditions and resulting impact on primary production and fisheries biomass.

5 Conclusions

For the Rhodes gyre area the changing climatic conditions form the greatest challenge: the current high productivity system is based on occasional deep overturning of the water column in the center of the Rhodes gyre, caused mainly by long, cold winters, resulting in high nutrient concentrations in the euphotic zone and a highly productive area in the otherwise oligotrophic Eastern Mediterranean. As air temperatures increase from ~17°C in 2009 to 22°C by the year 2100 in this area, winters are not cold enough anymore to cause the surface layer density to become higher than that of the Levantine Deep Water layer found below 200m. Thus, deep overturning of the water column declines with increasing air temperatures, and (in these simulations) stops from 2060 onwards under the RCP8.5 (business as usual) scenario. This causes a strong decline in surface nutrient concentrations, and thus phytoplankton biomass. Species composition shifts from microphytoplankton (diatoms, dinoflagellates) to nano- and picophytoplankton in the top mixed layer, as smaller organisms are better adapted to taking up nutrients in a low-nutrient environment. As such, the center of the Rhodes gyre starts to resemble the conditions now found on the periphery of the system. Acidification impacts were observed but generally did not influence the dominant climate stressor signal.

The combination of climate change and fishing pressure caused higher trophic level changes of the order of 30% (RCP4.5 or Paris agreement scenario) to 40 % (RCP8.5 or business as usual scenario) by the end of the 21st century. Fishing and climate change pressures were additive in our study for some species, while synergistic for others. In particular the biomass stocks of anchovy and sardines (the main targeted species in the system) showed synergistic and additive responses, respectively. Reduced fishing pressure only had a limited beneficial effect on commercial stock levels, indicating that positive management action on local fisheries will not be enough to offset the huge impact of

the warming climate, which already occurs under a medium emissions scenario (RCP4.5). These climatic changes represent a serious and sustained pressure, which will interact with other economic and sociological pressures, potentially in an extremely negative way. Therefore, a fully spatial ecosystem study is recommended for the Mediterranean, including a full representation of the thermohaline circulation and socio-economic studies into societies dependent on its resources.

Acknowledgements

The authors would like to thank Kostas Tsiaras from the Hellenic Centre of Marine Research (HCMR, Greece) for providing lower trophic level parameter settings from their Eastern Mediterranean ERSEM model. This research was supported by the European Commission, Horizon 2020 Framework Programme OCEAN CERTAIN (grant no. 603773).

Literature Cited

Baretta JW, Ebenhöh W, Ruardij P (1995) The European Regional Seas Ecosystem Model: A complex marine ecosystem model. Neth J Sea Res 33:233-246

Beecham J, Bruggeman J, Aldridge J, Mackinson S (2016) Couplerlib: a metadata-driven library for the integration of multiple models of higher and lower trophic level marine systems with inexact functional group matching. Geosci Model Dev 9(3):947-964. doi:10.5194/gmd-9-947-2016

Beuvier J, Brossier CL, Béranger K, Arsouze T, Bourdallé-Badie R, Deltel C, Drillet Y, Drobinski P, Ferry N, Lyard F (2012) MED12, Oceanic component for the modelling of the regional Mediterranean earth system. Mercator Ocean Quarterly Newsletter 46, hal-01138958

Casini M, Hjelm J, Molinero JC, Lövgren J, Cardinale M, Bartolino V, Belgrano A, Kornilovs G (2009). Trophic cascades promote threshold-like shifts in pelagic marine ecosystems. Proceedings of the National Academy of Sciences, 106(1):197-202

Christensen V, Pauly D (1992) ECOPATH II – a software for balancing steady-state ecosystem models and calculating network characteristics. Ecol Model 61:169-185. doi: 10.1016/0304-3800(92)90016-8

Christensen V, Walters CJ, Pauly D (2005) Ecopath with Ecosim: a User's Guide. Fisheries Centre, University of British Columbia, Vancouver. November 2005 edition, 154 p. (www.ecopath.org)

Coll M, Piroddi C, Steenbeek J, Kaschner K, Lasram FBR, Aguzzi J, Ballesteros E, Bianchi CN, Corbera J, Dailianis T, Danovaro R (2010) The biodiversity of the Mediterranean Sea: estimates, patterns, and threats. *PloS one 5*(8):e11842

Coll M, Libralato S (2012) Contributions of food web modelling to the ecosystem approach to marine resource management in the Mediterranean Sea. Fish and Fisheries, 13:60-88 DOI: 10.1111/j.1467-2979.2011.00420.x

Colloca F, Scarcella G, Libralato S (2017) Recent Trends and Impacts of Fisheries Exploitation on Mediterranean Stocks and Ecosystems. Front Mar Sc 4:244, DOI: 10.3389/fmars.2017.00244

Colonese AC, Mannino MA, Mayer DBY, Fa DA, Finlayson JC, Lubell D, Stiner MC (2011) Marine mollusc exploitation in Mediterranean prehistory: an overview. Quaternary international 239(1-2):86-103 DOI: 10.1016/j.quaint.2010.09.001

Corrales X, Coll M, Ofir E. et al. (2018) Future scenarios of marine resources and ecosystem conditions in the Eastern Mediterranean under the impacts of fishing, alien species and sea warming. Sci Rep 8:14284. DOI: 10.1038/s41598-018-32666-x

Cramer W, Guiot J, Fader M, Garrabou J, Gattuso J-P et al. (2018) Climate change and interconnected risks to sustainable development in the Mediterranean. Nat Clim Change 8(11):972 - 980. DOI: 10.1038/s41558-018-0299-2

D'Alelio D, Rampone S, Cusano LM, Morfino V, Russo L, Sanseverino N, Cloern JE, Lomas MW (2020) Machine learning identifies a strong association between warming and reduced primary productivity in an oligotrophic ocean gyre. Scientific reports, 10(1):1-12

Demirov E, Pinardi N (2002) Simulation of the Mediterranean Sea circulation from 1979 to 1993: Part I. The interannual variability. J Mar Syst 33:23-50. DOI: 10.1016/S0924-7963(02)00051-9

DOE (1994) Handbook of methods of the various parameters of the carbon dioxide system in seawater. Dickson AG & Goyet C (eds) ORNL/CDIAC-74, p. 25-26.

Ediger D & Yilmaz A (1996) Characteristics of deep chlorophyll maximum in the north-eastern Mediterranean with respect to environmental conditions. J Mar Syst 9: 291-303

Ediger D, Tuğrul S, Yilmaz A (2004) Vertical profiles of particulate organic matter and its relationship with chlorophyll-a in the upper layer of the NE Mediterranean Sea. J Mar Syst 55:311– 326 DOI:10.1016/j.jmarsys.2004.09.003

Galil BS (2009) Taking stock: inventory of alien species in the Mediterranean sea. Biol Invasions 11**:** 359–372, DOI: 10.1007/s10530-008-9253-y

Galil BS (2012) Truth and consequences: the bioinvasion of the Mediterranean Sea. Integr Zool, 7(3):299-311

Galil BS & Goren M (2014) Metamorphoses: bioinvasions in the Mediterranean Sea. In The Mediterranean Sea (pp. 463-478). Springer, Dordrecht.

Giorgi F, Lionello P (2008) Climate change projections for the Mediterranean region. Global Planet Change 63(2-3):90-104 DOI:10.1016/j.gloplacha.2007.09.005.

Herrmann M, Estournel C, Déqué M, Marsaleix P, Sevault F, Somot S (2008) Dense water formation in the Gulf of Lion shelf: impact of atmospheric interannual variability and climate change. Cont Shelf Res 28:2092–2112, DOI: 10.1016/j.csr.2008.03.003

Hopwood MJ, Sanchez N, Polyviou D, Leiknes Ø, Gallego-Urrea JA, Achterberg EP, Ardelan MV, Aristegui J, Bach L., Besiktepe S, Heriot Y, Kalantzi I, Terbıyık Kurt T, Santi I, Tsagaraki TM, Turner D (2020) Experiment design and bacterial abundance control extracellular H_2O_2 concentrations during four series of mesocosm experiments. Biogeosciences, 17:1309–1326. DOI: 10.5194/bg-17-1309-2020

IPCC (2014) Climate change 2014: A synthesis report. Contribution of working groups I, II and III to the Fifth Assessment Report of the Intergovernmental Panel on Climate Change. Geneva, Switzerland, IPCC, 151 p., ISBN: 978-92-9169-143-2

Ji BY, Sandwith ZO, Williams WJ, Diaconescu O, Ji R, Li Y, Van Scoy E, Yamamoto-Kawai M, Zimmermann S, Stanley RH (2019) Variations in rates of biological production in the Beaufort Gyre as the Arctic changes: Rates from 2011 to 2016. J Geophys Res, C, Oceans, 124(6):3628-3644

Katsanevakis S, Tempera F, Teixeira H (2016) Mapping the impact of alien species on marine ecosystems: the Mediterranean Sea case study. Diversity and Distributions, 22(6):694-707

de Kok J-L, Viaene P, Vermeiren K, Van der Meulen M, Tiller R, Ardelan M, Bailey J, Thorpe R, Beecham J, Van Leeuwen SM, Thingstad F, Tsagaraki TM, Richards R, Bizsel C, Salgado H, **2016**, "*Integrating scientific knowledge, data and stakeholder perceptions for decision support*", Conference: International Congress on Environmental Modelling and Software, At Toulouse, France, Volume: 7

Kubin E, Poulain, P-M, Mauri E, Menna M, Notarstefano G (2019) Levantine Intermediate and Levantine Deep Water Formation: An Argo Float Study from 2001 to 2017. Water 11(9):1781. DOI: 10.3390/w11091781

Lascaratos A, Williams RG, Tragou E (1993) A mixed layer study of the formation of Levantine intermediate water. J Geophys Res Oceans 98(C8):14739-14749

Letscher RT, Primeau F, Moore JK (2016) Nutrient budgets in the subtropical ocean gyres dominated by lateral transport. Nature Geoscience, 9(11):815-819.

Malanotte-Rizzoli P, Manca BB., Ribera d'Alcala M, Theocharis A, Brenner S, Budillon G, Ozsoy E (1999) The Eastern Mediterranean in the 80s and in the 90s: the big transition in the intermediate and deep circulations. Dyn Atmos Oceans 29:365–395 PII: S0377- 0265_99.00011-1

722 Mannino AM, Balistreri P, Deidun A (2017) The marine biodiversity of the Mediterranean Sea in a
723 changing climate: the impact of biological invasions. Mediterranean identities-environment, society,
724 culture, pp.101-127 DOI: http://dx.doi.org/10.5772/intechopen.6921

725 Mazzocchi MG, Christou ED, Fragopoulu N, Siokou-Frangou I (1997) Mesozooplankton distribution
726 from Sicily to Cyprus (Eastern Mediterranean): I. General aspects. Oceanol Acta 20(3):521 – 535

727 Megalofonou P, Damalas D (2012) Discovering where bluefin tuna, Thunnus thynnus, might go: Using
728 environmental and fishery data to map potential tuna habitat in the eastern Mediterranean Sea. Scienta
729 Marina 76(4):691-704, DOI: 10.3989/scimar.03679.26A

730 Menna M & Poulain PM (2010) Mediterranean intermediate circulation estimated from Argo data in
731 2003–2010. Ocean Science 6(1):331-343. DOI: 10.5194/os-6-331-2010

732 Moullec F, Barrier N, Drira S, Guilhaumon F, Marsaleix P, Somot S, Ulses C, Velez L, Shin Y-J, (2019a)
733 An End-to-End Model Reveals Losers and Winners in a Warming Mediterranean Sea. Front Mar Sci
734 6:345. DOI: 10.3389/fmars.2019.00345

735 Moullec F., Velez L., Verley P., Barrier N., Ulses C., Carbonara P., Esteban A., Follesa C., Gristina M.,
736 Jadaud A., Ligas A., López Díaz E., Maiorano P., Peristeraki P., Spedicato M.T., Thasitis I., Valls M.,
737 Guilhaumon F, Shin Y-J (2019b) Capturing the big picture of Mediterranean marine biodiversity with an
738 end-to-end model of climate and fishing impacts. Prog Oceanogr 178:102179. DOI:
739 10.1016/j.pocean.2019.102179

740 Murphy S, Richards LA, Wimp GM (2020) Arthropod interactions and responses to disturbance in a
741 changing world. Frontiers in Ecology and Evolution, 8:93.

742 Niiranen S, Yletyinen J, Tomczak MT, Blenckner T, Hjerne O, MacKenzie BR, Müller-Karulis B,
743 Neumann T, Meier HM (2013) Combined effects of global climate change and regional ecosystem drivers
744 on an exploited marine food web. Global change biology, 19(11):3327-3342

745 Olli K (1999) Diel vertical migration of phytoplankton and heterotrophic flagellates in the Gulf of Riga, J
746 Mar Sys, 23 (1-3):145-163, DOI: 10.1016/S0924-7963(99)00055-X

747 Pinardi N & Masetti E (2000) Variability of the large scale general circulation of the Mediterranean Sea
748 from observations and modelling: a review. Palaeogeogr Palaeoclimatol Palaeoecol 158:153-173

749 Poulos SE, Drakopoulos PG (2001) A reassessment of the Mediterranean river runoff. Rapp Comm Int
750 Mer Medit 36:76

751 Powley HR, Van Capellen P, Krom MD (2017) Nutrient cycling in the Mediterranean Sea: the key to
752 understanding how the unique marine ecosystem functions and responds to anthropogenic pressures. In
753 Fuerst-Bjelis B (eds) Mediterranean Identities - Environment, Society, Culture. DOI:
754 10.5772/intechopen.70878

755 Reid PC, Battle EJV, Batten SD, Brander KM (2000) Impacts of fisheries on plankton community
756 structure. ICES J Mar Sci 57(3):495-502

757 Robinson AR, Leslie WG, Theocharis A, Lascaratos A (2001) Mediterranean Sea circulation. Ocean
758 Currents, 1:19, DOI: 10.1006/rwos.2001.0376

759 Roether W, Manca BB, Klein B, Bregant D, Georgopoulos D, Beitzel V, Kovačević V, Luchetta A (1996)
760 Recent changes in eastern Mediterranean deep waters. Science 271(5247):333-335

761 Serpetti N, Baudron AR, Burrows MT, Payne BL, Helaouet P, Fernandes PG, Heymans JJ (2017) Impact
762 of ocean warming on sustainable fisheries management informs the Ecosystem Approach to Fisheries.
763 Scientific reports 7(1):1-15

764 Staker RD & Bruno SF (1980) Diurnal Vertical Migration in Marine Phytoplankton. Botanica Marina
765 23(3):167-172. DOI:10.1515/botm.1980.23.3.167

766 Salihoglu I, Saydam C, Bastrurk O, Yilmaz K, Gocmen D, Hatipoglu E, Yilmaz A (1990) Transport and
767 distribution of nutrients and chlorophyll-a by mesoscale eddies in the Northeastern Mediterranean. Mar
768 Chem 29:375-390

769 Shaltout M & Omstedt A (2014) Recent sea surface temperature trends and future scenarios for the
770 Mediterranean Sea. Oceanologia 56(3):411-443, DOI:10.5697/oc.56-3.411

771 Siokou-Frangou I, Gotsis-Skreta O, Christou E, Pagou K (1999) Plankton characteristics in the Aegean,
772 Ionian and NW Levantine Seas. In Malanotte-Rizzoli P & Eremeev VN (eds) The Eastern Mediterranean
773 as a laboratory basin for assessment of contrasting ecosystems, Kluwer Acad. Press, Dordrecht, doi:
774 10.1007/978-94-011-4796-5_15

775 Siokou-Frangou I, Christaki U, Mazzocchi MG, Montresor M, Ribera d'Alcalá M, Vaqué D, Zingone A
776 (2010) Plankton in the open Mediterranean Sea: a review. Biogeosciences 7:1543–1586, DOI:
777 10.5194/bg-7-1543-2010

778 Siokou-Frangou I, Christou ED, Fragopoulu N, Mazzocchi MG (1997) Mesozooplankton distribution
779 from Sicily to Cyprus (Eastern Mediterranean): II. Copepod assemblages. Oceanol Acta 20(3):537-548

780 Skliris N, Marsh R, Josey SA, Good SA, Liu C, Allan RP (2014) Salinity changes in the World Ocean
781 since 1950 in relation to changing surface freshwater fluxes. Clim Dyn 43:709–736, DOI:
782 10.1007/s00382-014-2131-7

783 Steenbeek J, Buszowski J, Christensen V, Akoglu E, Aydin K, Ellis N, Felinto D, Guitton J, Lucey S,
784 Kearney K, Mackinson S, Pan M, Platts M, Walters C (2015) Ecopath with Ecosim as a model-building
785 toolbox: source code capabilities, extensions, and variations**.** Ecol Modell 319:178-189 doi:
786 10.1016/j.ecolmodel.2015.06.031

787 Taherzadeh N, Bengfort M, Wirtz KW (2019) A trait-based framework for explaining non-additive
788 effects of multiple stressors on plankton communities. Frontiers in Marine Science, 6:351

789 Taylor KE, Stouffer RJ, Meehl GA (2012) An Overview of CMIP5 and the Experiment Design. Bull Am
790 Met Soc 93(4):485-498 doi: 10.1175/BAMS-D-11-00094.1

791 Teruzzi A, Bolzon G, Salon S, Lazzari P, Solidoro C, Cossarini G (2018) Assimilation of coastal and open
792 sea biogeochemical data to improve phytoplankton simulation in the Mediterranean Sea. Ocean Model
793 132:46-60, DOI: 10.1016/j.ocemod.2018.09.007

794 Thomas MK, Aranguren-Gassis M, Kremer CT, Gould MR, Anderson K, Klausmeier CA, Litchman E
795 (2017) Temperature–nutrient interactions exacerbate sensitivity to warming in phytoplankton. Global
796 Change Biology, 23(8):3269-3280

797 Tsagarakis K, Coll M, Giannoulaki M, Somarakis S, Papaconstantinou C, Machias A (2010) Food-web
798 traits of the North Aegean Sea ecosystem (Eastern Mediterranean) and comparison with other
799 Mediterranean ecosystems. Estuar Coast Shelf Sci 88(2):233-248

800 van der Molen J, Aldridge JN, Coughlan C, Parker ER, Stephens D, Ruardij P (2013) Modelling marine
801 ecosystem response to climate change and trawling in the North Sea. Biogeochemistry 113(1–3):213-236
802 doi:10.1007/s10533-012-9763-7.

803 van Leeuwen SM, le Quesne W, Parker ER (2016) Potential future fisheries yields in shelf waters: a model
804 study of the effects of climate change and ocean acidification. Biogeosciences 13(2): 441-454, DOI:
805 10.5194/bg-13-441-2016

806 Vichi M, Cossarini G, Gutierrez Mlot E, Lazzari P, Lovato T, Mattia G, Masina S, McKiver W, Pinardi N,
807 Solidoro C, Zavatarelli M (2013) The Biogeochemical Flux Model (BFM): Equation Description and User
808 Manual. BFM version 5 (BFM-V5) Release 1.0; BFM Report series N. 1. March 2013, Bologna, Italy,
809 http://bfm-community.eu, 87 p.

810 Vidussi F, Claustre H, Manca BB, Luchetta A, Marty J-C (2001) Phytoplankton pigment distribution in
811 relation to upper thermocline circulation in the eastern Mediterranean Sea during winter. J Geoph Res
812 Oceans 106(C9):19,939-19,956 DOI: 10.1029/1999JC000308

813 Wirtz K & Smith SL (2020) Vertical migration by bulk phytoplankton sustains biodiversity and nutrient
814 input to the surface ocean. Scientific reports, 10(1):1-12

815 Wu P & Haines K (1996) Modeling the dispersal of Levantine Intermediate Water and its role in
816 Mediterranean deep water formation. J Geoph Res Oceans 101(C3):6591-6607.

Yilmaz A, Souvermezoglou E, Ediger D (2007) Climate change impacts on ecosystems: the Rhodes Gyre case. Rapp Comm Int Mer Médit 38

Zhang Y, Mahowald N, Scanza R, Journet E, Desboeufs K, Albani S, Kok J, Zhuang G, Chen Y, Cohen DD, Paytan A, Patey MD, Achterberg EP, Engelbrecht JP and Fomba KW (2015) Modeling the global emission, transport and deposition of trace elements associated with mineral dust. Biogeosciences 12:5771–5792

Tables

Table 1: species/families included in the Rhodes gyre setup of the Ecopath with Ecosim model. Based on the Aegean model of Tsagarakis et al. (2010).

	Functional group name	Production/ Biomass [1/y]		Functional group name	Production/ Biomass [1/y]
1	Phytoplankton	117.30	*13*	Adult sardine	1.20
2	Ciliates	258.85	*14*	Horse mackerels	1.08
3	Mesozooplankton	29.19	*15*	Mackerels	0.97
4	Macrozooplankton	21.07	*16*	Other Small pelagic fishes	0.75
5	Jellyfish & M. leidyi	4.84	*17*	Medium pelagic fishes	0.61
6	Squids	2.60	*18*	Large pelagic fishes	0.34
7	Hake	0.75	*19*	Loggerhead turtle	0.16
8	Benthopelagic fishes	1.25	*20*	Seabirds	4.78
9	Picarels & bogue	1.69	*21*	Dolphins	0.08
10	Juv. anchovy	2.25	*22*	Detritus	
11	Adult anchovy	1.37	*23*	Discards	
12	Juv. sardine	1.62			

Table 2: The different scenarios used in the study, and their abbreviations. The light blue color refers to scenarios with standard fishing pressure, while the mid-blue and dark-blue colors refer to scenarios with low and high fishing pressure, respectively. Note that the reference scenario has the current fishing pressure which is above MSY levels.

Scenario Name	Description
Reference	Repeat of the meteorology from 1979-2008, atmospheric pCO2 values constant from 2008 onwards
CC1	Meteorological conditions from the RCP4.5 pathway (Paris agreement), atmospheric pCO2 values constant from 2008 onwards
CC2	Meteorological conditions from the RCP8.5 pathway (business as usual), atmospheric pCO2 values constant from 2008 onwards
OA1	Repeat of the meteorology from 1979-2008, atmospheric pCO2 values increasing according to the RCP4.5 pathway (Paris agreement)
OA2	Repeat of the meteorology from 1979-2008, atmospheric pCO2 values increasing according to the RCP8.5 pathway (business as usual)
CC1OA1	Meteorological conditions and atmospheric pCO2 values according to the RCP4.5 pathway (Paris agreement)
CC2OA2	Meteorological conditions and atmospheric pCO2 values according to the RCP8.5 pathway (business as usual)

LF	Low fishing pressure (MSY) and repeat of the meteorology from 1979-2008, atmospheric pCO2 values constant from 2008 onwards
CC1LF	CC1 scenario combined with MSY fishing pressure
CC2LF	CC2 scenario combined with MSY fishing pressure
CC1OA1LF	Full RCP4.5 pathway combined with MSY fishing pressure
CC2OA2LF	Full RCP8.5 pathway combined with MSY fishing pressure
HF	High fishing pressure (MSY++) and repeat of the meteorology from 1979-2008, atmospheric pCO2 values constant from 2008 onwards
CC1HF	CC1 scenario combined with MSY++ fishing pressure
CC2HF	CC2 scenario combined with MSY++ fishing pressure
CC1OA1HF	CC1OA1 scenario combined with MSY++ fishing pressure
CC2OA2HF	CC2OA2 scenario combined with MSY++ fishing pressure

Table 3: The breakup of the simulated period into 30-year blocks.

1958-1978	Spin-up time	
1979-2008	Current conditions	Reflecting the state which the current economic use of the resources is based on
2009-2038	Future block 1	Immediate future prediction
2039-2068	Future block 2	Intermediate future prediction
2069-2098	Future block 3	Long-term future prediction

Table 4: higher trophic level changes. Averaged values for 2080-2099 were compared for the different scenarios.

Percentage change	Ref LF vs CC1 LF	Ref LF vs CC2 LF	Ref HF vs CC1 HF	Ref HF vs CC2 HF	Ref LF vs Ref HF	CC1 LF vs CC1 HF	CC2 LF vs CC2 HF
Anchovies	**-25.71**	**-40.00**	**-33.33**	**-47.37**	**-18.57**	**-26.92**	**-28.57**
Sardines	**-30.77**	**-38.46**	**-30.00**	**-40.00**	**-23.08**	**-22.22**	**-25.00**
Mackerel	**-32.22**	**-40.00**	**-29.20**	**-34.51**	**0.44**	**4.92**	**9.63**
Dolphins	**-31.43**	**-38.57**	**-32.40**	**-38.00**	**-10.71**	**-11.98**	**-9.88**

Figures

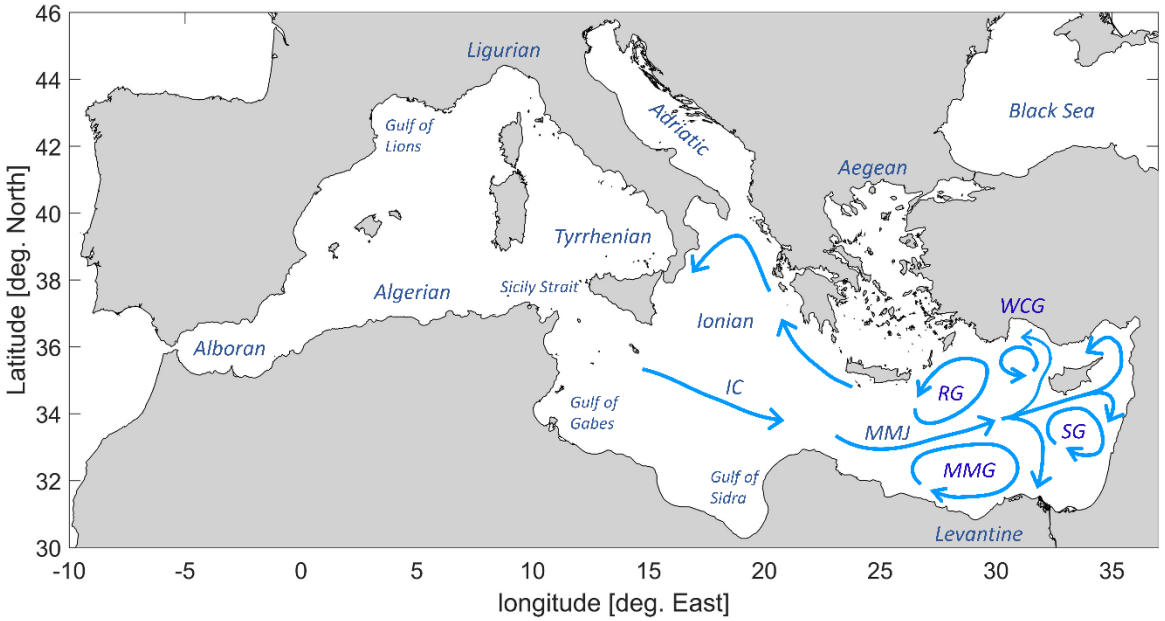

Figure 1: Schematic of the surface thermohaline circulation in the Eastern Mediterranean, including the main gyre system in the Levantine basin. Here IC is the Ionian Current, MMJ the Mid-Mediterranean Jet, RG the Rhodes Gyre, WCG the West Cyprus Gyre, MMG the Mersa-Matruh Gyre and SG the Shikmona GyreBased on Thorpe & Bigg (2000) and Malanotte-Rizzoli et al (1999).

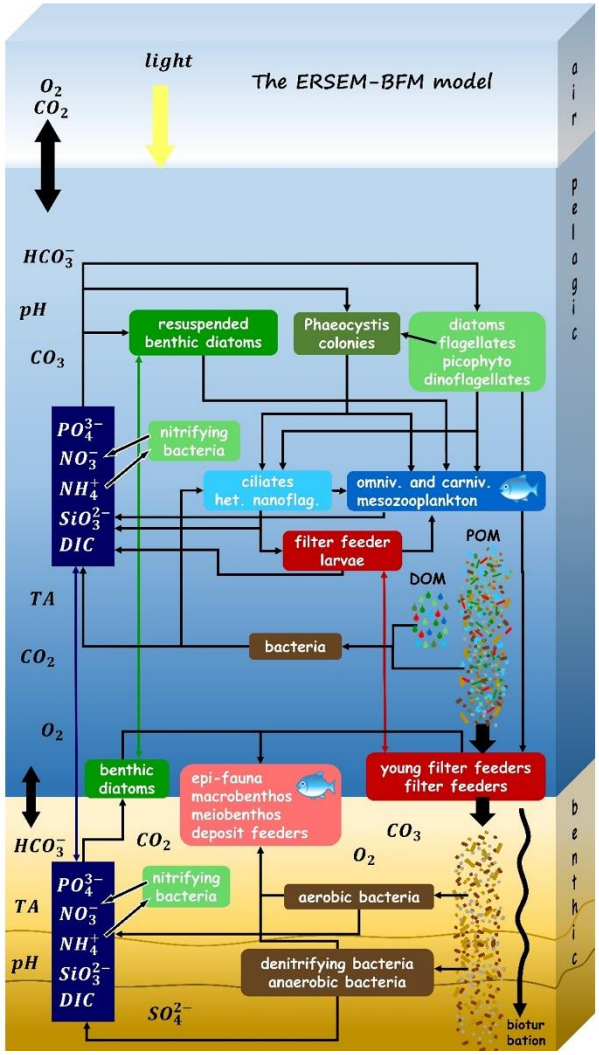
light
The ERSEM-BFM model
air
pelagic
benthic
O_2
CO_2
HCO_3^-
pH
CO_3
PO_4^{3-}
NO_3^-
NH_4^+
SiO_3^{2-}
DIC
TA
resuspended benthic diatoms
Phaeocystis colonies
diatoms flagellates picophyto dinoflagellates
nitrifying bacteria
ciliates het. nanoflag.
omniv. and carniv. mesozooplankton
filter feeder larvae
POM
DOM
bacteria
benthic diatoms
epi-fauna macrobenthos meiobenthos deposit feeders
young filter feeders filter feeders
aerobic bacteria
denitrifying bacteria anaerobic bacteria
SO_4^{2-}
biotur bation

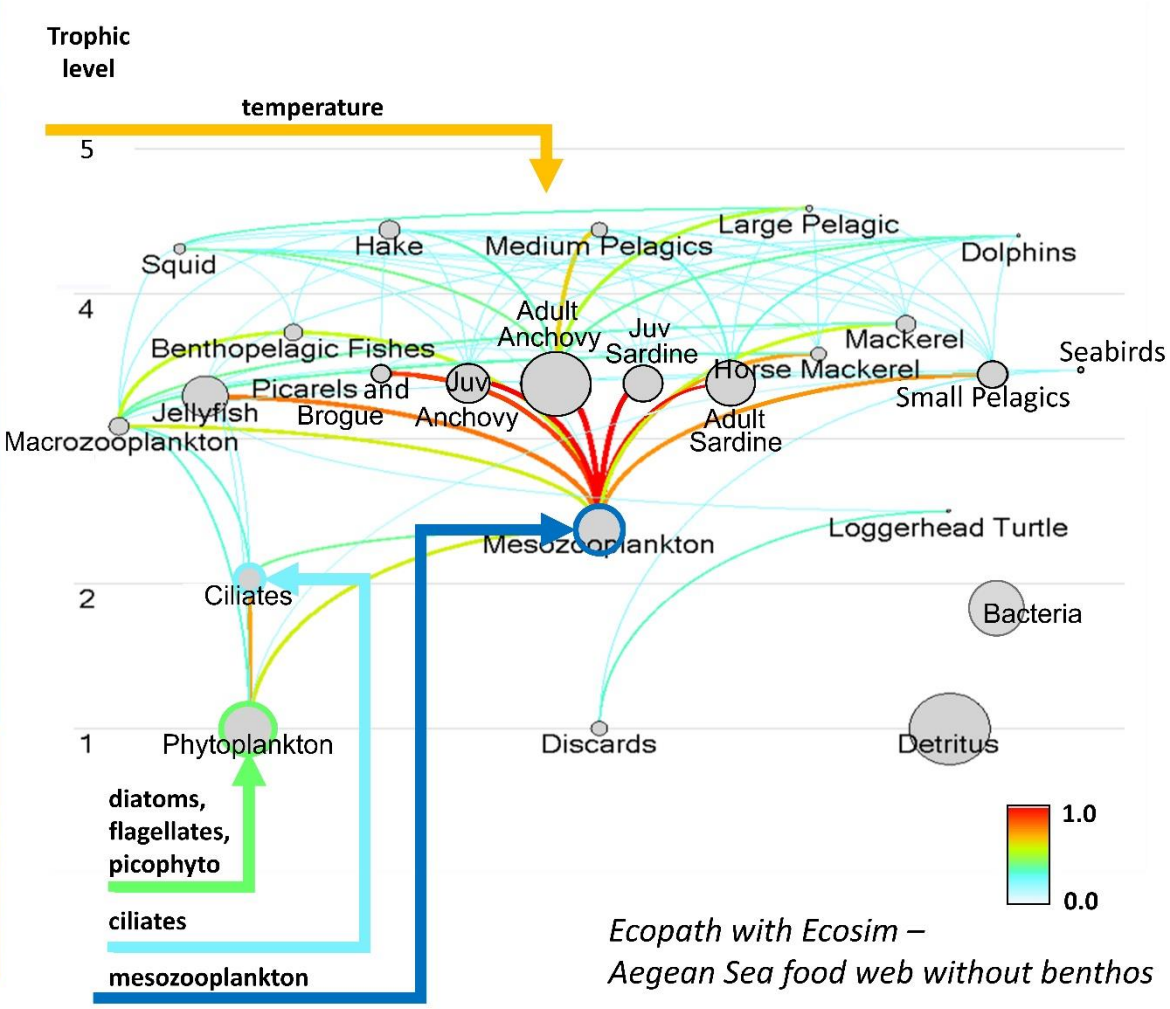
Trophic level
temperature
5
4
2
1
Squid
Hake
Medium Pelagics
Large Pelagic
Dolphins
Benthopelagic Fishes
Adult Anchovy
Juv Sardine
Mackerel
Seabirds
Horse Mackerel
Small Pelagics
Picarels and Brogue
Juv Anchovy
Jellyfish
Adult Sardine
Macrozooplankton
Mesozooplankton
Loggerhead Turtle
Ciliates
Bacteria
Phytoplankton
Discards
Detritus
diatoms, flagellates, picophyto
ciliates
mesozooplankton
1.0
0.0
Ecopath with Ecosim –
Aegean Sea food web without benthos

Figure 2: the coupled model. ERSEM-BFM schematic (left) and the applied EwE food web (right). The arrows denote the linking, where time-dependent information from the lower trophic level model was fed into the higher trophic level model. The colour scale for EwE displays the normalized energy flow between species, while the grey circles indicate relative biomass. Here "Juv" stands for "juvenile". The benthic compartment of ERSEM-BFM was not used here.

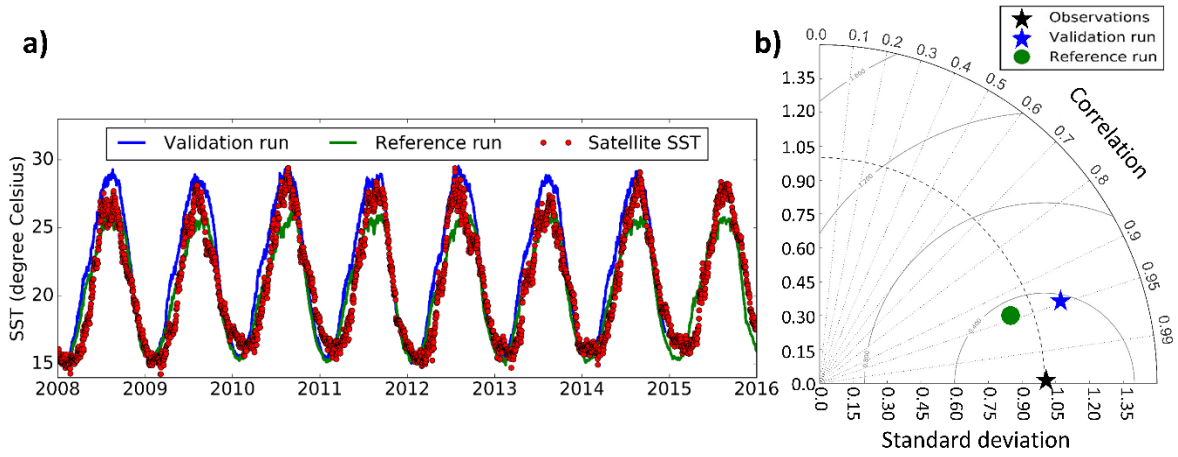

Figure 3: Comparison of modelled SST from the validation and reference runs with satellite SST observations at the chosen model location. a) direct comparison, b) Taylor diagram.

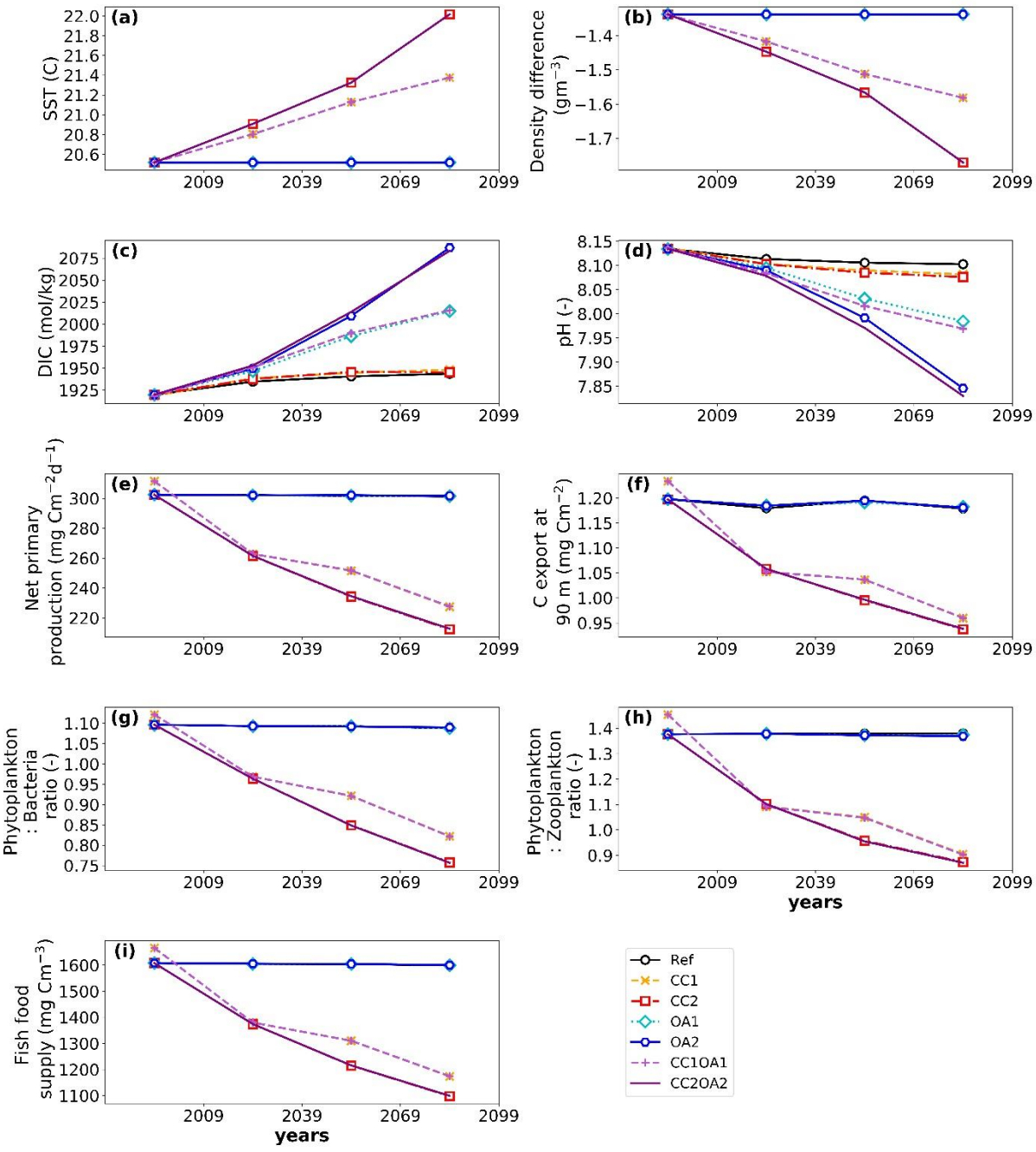

Figure 4: Results in 30-year averaged time blocks for all scenarios for the Rhodes gyre: a) sea surface temperature, b) density difference between the top and bottom layer, indicating strength of stratification, c) surface dissolved inorganic carbon concentration, d) surface pH, e) depth-integrated net primary production, f) carbon export below 90 m, g) biomass ratio of phytoplankton to pelagic bacteria integrated over the first 150m, h) biomass ratio of phytoplankton to zooplankton integrated over the first 150m and i) combined depth-integrated plankton biomass input into Ecopath with Ecosim, indicating available fish food. Here Ref stands for Reference (continued 1979-2008 conditions), CC stand for climate change (CC1: RCP4.5, CC2: RCP8.5) and OA for ocean acidification (OA1: pCO_2 of RCP4.5, OA2: pCO_2 of RCP8.5). For a full explanation of the scenario abbreviations see Table 2.

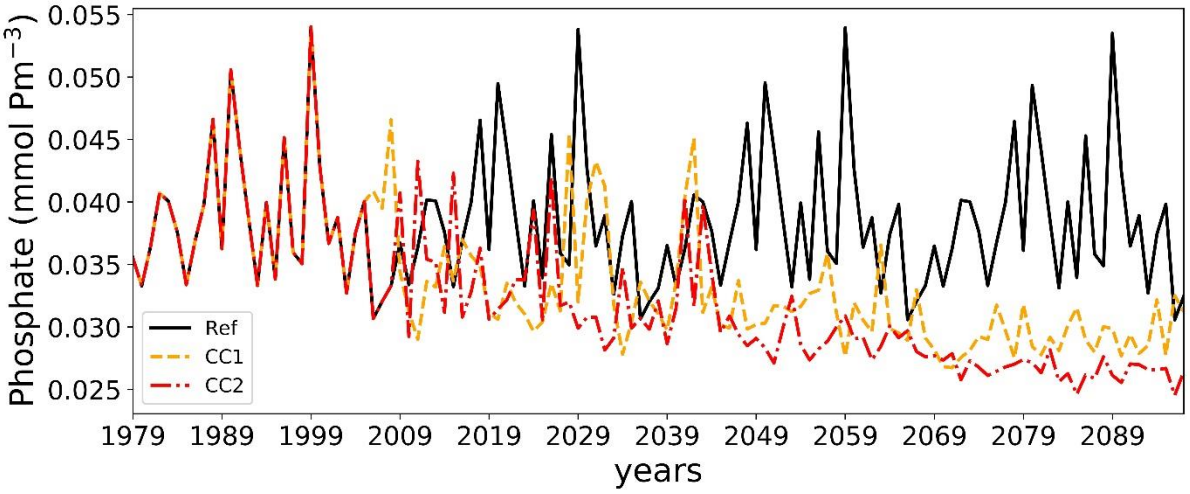

Figure 5:Surface phosphate levels (maximum per year) for the reference and climate stressor only scenarios. High levels of surface phosphate indicate deep overturning years.

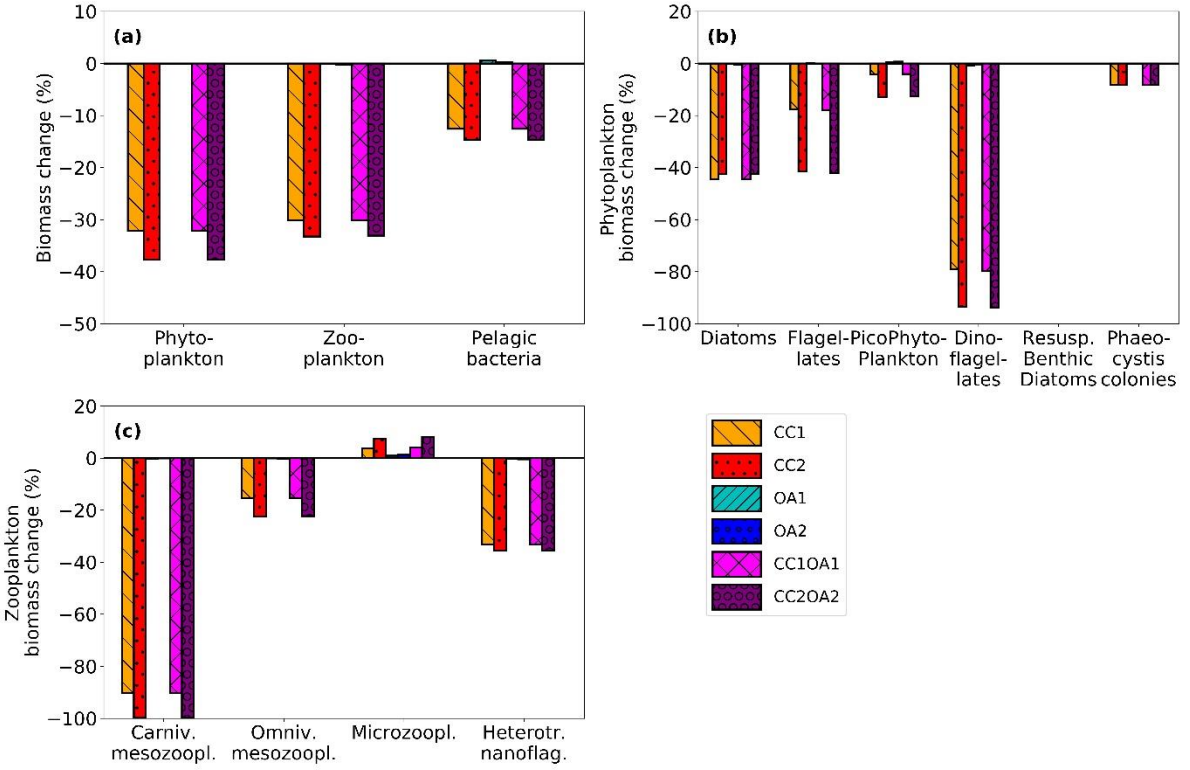

Figure 6: Predicted percentage changes in biomass for all scenario at the Rhodes gyre site for a) all main biomass groups, b) phytoplankton functional groups and c) zooplankton functional groups. Here Ref stands for Reference (continued 1979-2008 conditions), CC stand for climate change (CC1: RCP4.5, CC2: RCP8.5) and OA for ocean acidification (OA1: pCO_2 of RCP4.5, OA2: pCO_2 of RCP8.5). For a full explanation of the scenario abbreviations see Table 2. Benthic organisms and processes were not simulated at this deep site, and Phaeocystis levels were extremely low throughout.

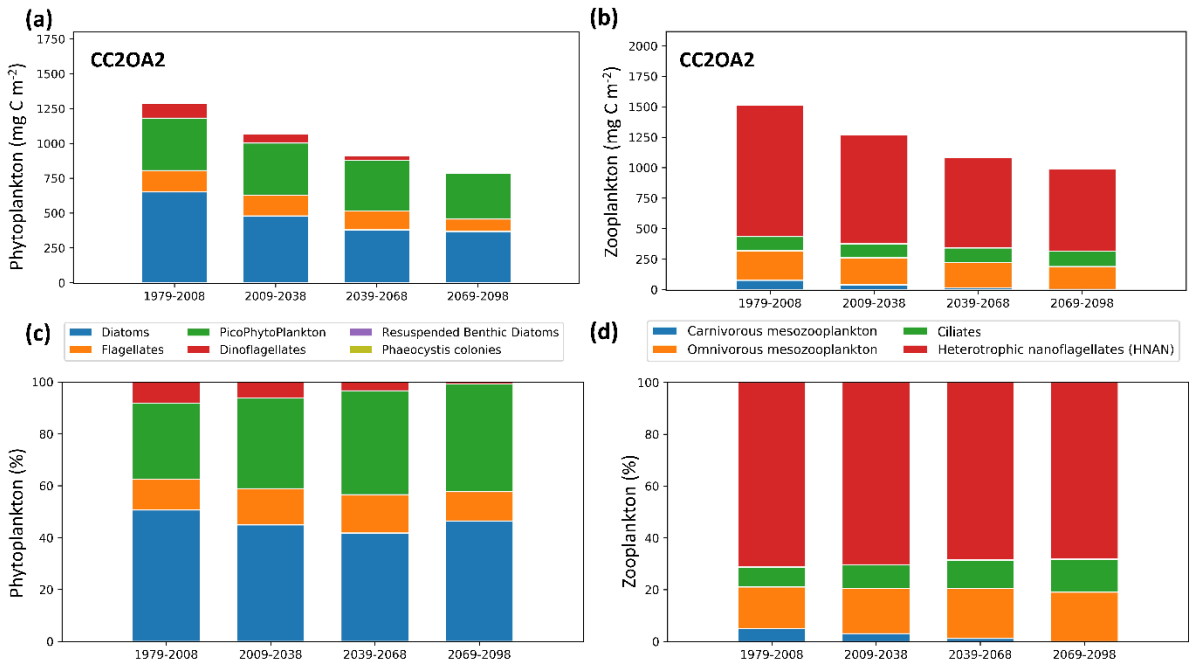

Figure 7: Plankton assemblages for the CC2OA2 scenario, for the 30-year intervals: a) Phytoplankton actual biomass values, b) zooplankton actual biomass values, c) phytoplankton percentage contribution by functional group, d) zooplankton percentage contribution by functional group, all depth-integrated values. Note that the first period (1979-2008) is equivalent to the reference scenario results.

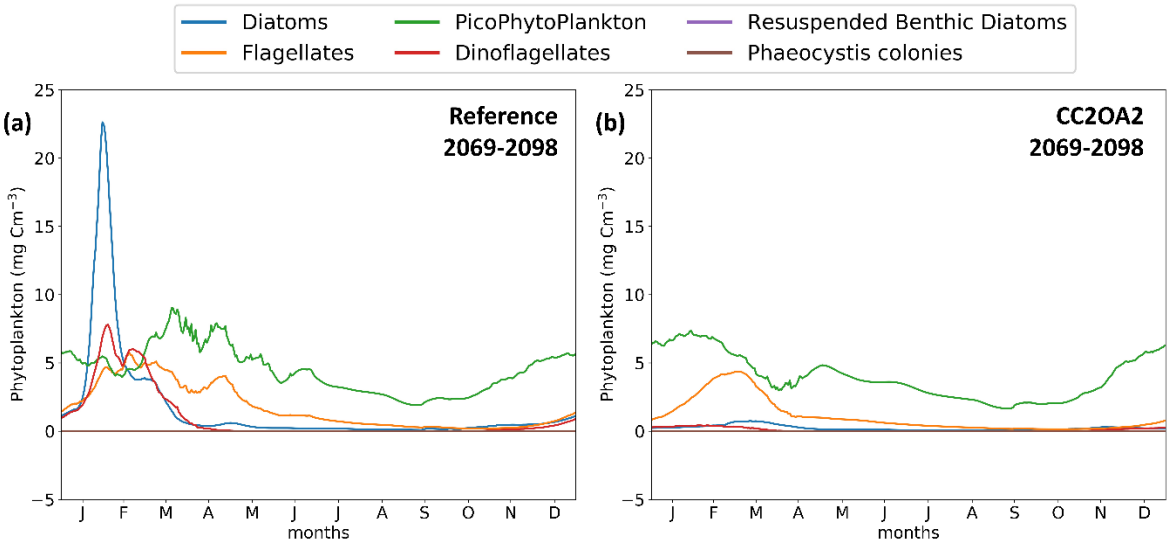

Figure 8: Seasonal signal of phytoplankton functional groups at the surface for the Rhodes gyre: a) the reference simulation and b) the CC2OA2 scenario (full RCP8.5 implementation). Note that negative values do not occur; the negative minimum range is displayed solely to highlight values close to 0.

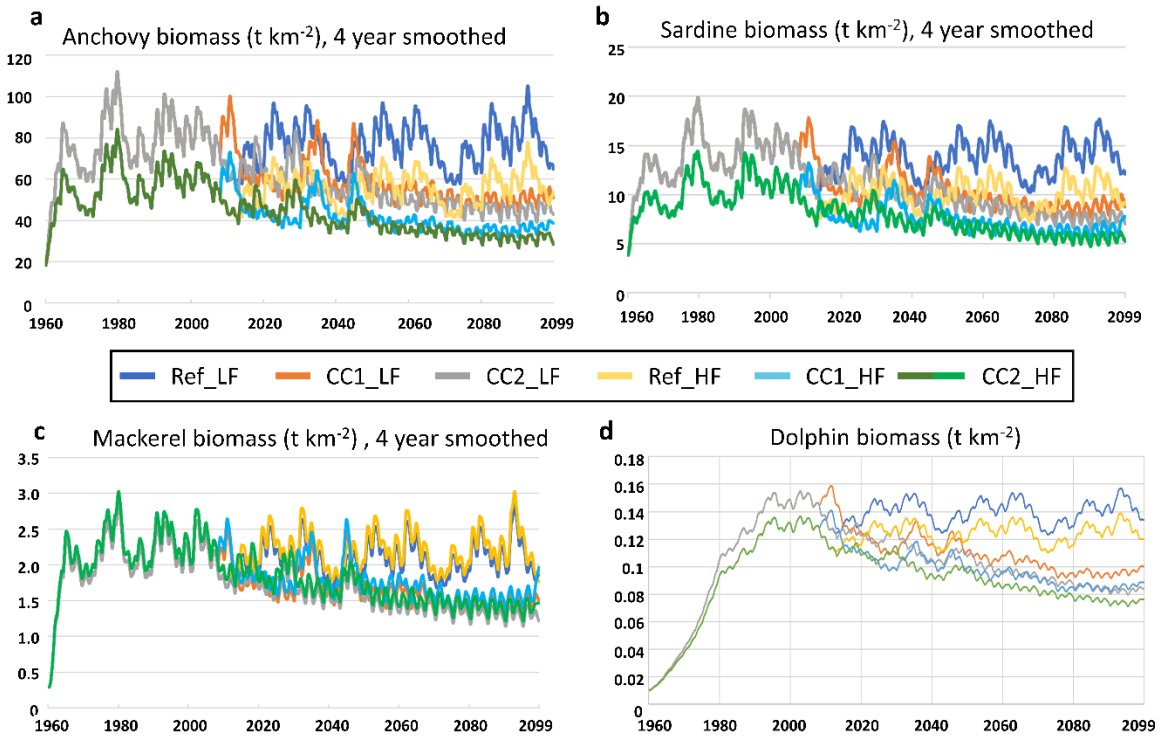

Figure 9: Biomasses (t km^{-2}) of a) anchovy (smoothed), b) sardines (smoothed), c) mackerel (smoothed) and d) dolphins in the climate change and reference scenarios for low and high fishing. Here Ref stands for Reference (continued 1979-2008 conditions), CC stand for climate change (CC1: RCP4.5, CC2: RCP8.5), OA for ocean acidification (OA1: pCO_2 of RCP4.5, OA2: pCO_2 of RCP8.5) and LF and HF for low (~MSY) and high fishing (2x current level), respectively. For a full explanation of the scenario abbreviations see Table 2.